

Single-Molecule Force Spectroscopy of a Tetraaryl Succinonitrile Mechanophore

Martijn van Galen, Jeya Prathap Kaniraj, Bauke Albada, and Joris Sprakel*

Cite This: *J. Phys. Chem. C* 2022, 126, 1215–1221

Read Online

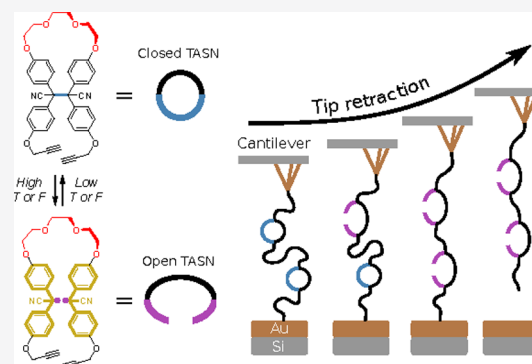
ACCESS |

Metrics & More

Article Recommendations

Supporting Information

ABSTRACT: Fluorescent damage reporters that use mechanochemical activation of a covalent bond to elicit an optical signal are emerging tools in material mechanics as a means to access the nanoscale distribution of forces inside materials under stress. A promising class of damage reporters are tetraaryl succinonitriles (TASN), whose mechanical activation results in stable fluorescent radical species. However, in-depth insights into the molecular mechanics of TASN activation are absent, precluding their use as quantitative mechanoprobes. Here we perform single-molecule force spectroscopy experiments to provide these insights. We use a bridged version of the TASN unit, embedded in multi-mechanophore polymer, to enable multiplexed mechanochemical measurements at the single-molecule level. Our experiments reveal that TASN activates at surprisingly low forces and short time scales compared to other covalent mechanophores. These results establish TASN as a promising candidate for reporting the lower end of relevant forces in material mechanics.



The mechanical failure of materials, manifested macroscopically as catastrophic fracture or yielding, invariably commences by the rupture of cohesive bonds at the nanoscale. Direct measurement and visualization of nanoscale bond scission phenomena have recently become possible through the development and use of optically responsive mechanophores: small molecules that undergo a force-induced mechanochemical transition, for example, the scission of a labile bond, to an optically active state. When anchored into a polymeric material of interest, stresses applied to the polymers transfer to the mechanophores. Once a threshold force on a single mechanophore is exceeded, activation of the reporter can be detected optically by either absorption,^{1–4} mechanoluminescence,^{5,6} or fluorescence.^{1,7,8} This can provide a qualitative picture of where damage processes occur and to what extent. Making these results quantitative requires careful calibration, as was recently reported for spiropyran mechanophores⁹ and, ideally, detailed insights into the molecular kinetics of mechanochemical activation for the mechanophore of interest. To date, only very few optical mechanophores have been quantitatively scrutinized at the molecular level, spiropyran being the notable exception.¹⁰

Tetraaryl succinonitriles (TASN) have emerged as promising candidates for damage reporting.^{11–14} Mechanophores of this class consist of a central labile succinonitrile bond flanked by a total of four aromatic moieties (Figure 1a). When TASN molecules are placed under tension, the labile succinonitrile bond cleaves homolytically, resulting in two molecules that feature a strongly fluorescent and stable radical.¹¹ While mechanophore activation is often irreversible, e.g., for

dioxetanes^{6,15,16} and Diels–Alder adducts of anthracenes,^{17,18} TASN dissociation, like for spiropyran, is reversible.¹³ Radical recombination can lead to reformation of the original molecule. This reversibility is advantageous for its use as a damage reporter, as it allows for the repeated observation of many damage events over extended periods of time.

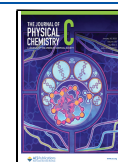
Because these binary optical damage reporters only activate when the local force exceeds a threshold value, interpreting optical damage assays in materials requires knowledge of the rupture force and underlying mechanochemical reaction kinetics and ideally access to reporters that span a range of threshold forces. These insights are absent for TASN as reports have so far relied on qualitative means to activate the central labile bond, such as grinding.¹¹

In this paper we use single-molecule force spectroscopy to perform a mechanical characterization of TASN mechanophores to investigate its potential as a fluorescent damage reporter. To ensure ample statistics during these measurements, we first synthesize a bridged version of the TASN molecule, which is incorporated into a multi-mechanophore polymer. We find that TASN activation occurs at lower forces and on shorter time scales as compared to other commonly

Received: October 27, 2021

Revised: December 21, 2021

Published: January 6, 2022



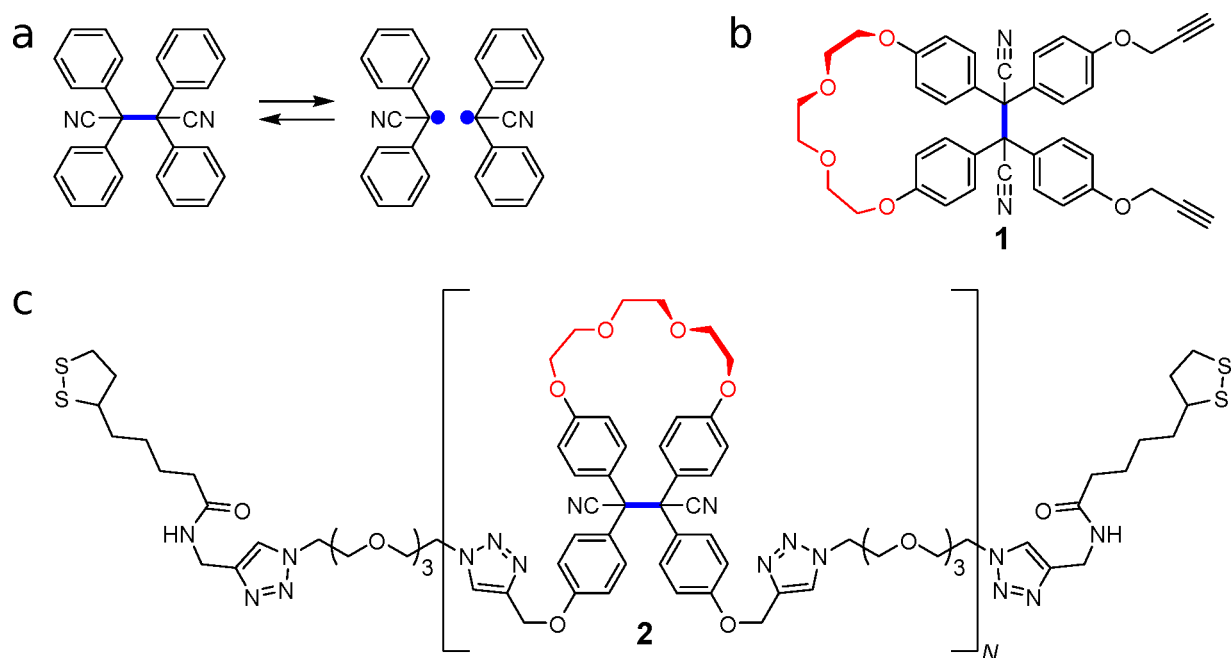


Figure 1. (a) Structure of tetraphenyl succinonitrile (TPSN) which can open and close reversibly under mechanical triggers, yielding two fluorescent radical species. The mechanically active bond is shown in blue. (b) Bridged tetraaryl succinonitrile (TASN) mechanophore **1**, with the triethylene glycol bridge shown in red. (c) Chemical structure of the bridged mechanophore incorporated in an ethylene glycol polymer **2**, capped on either end by lipoic acid groups for anchoring on gold-coated surfaces.

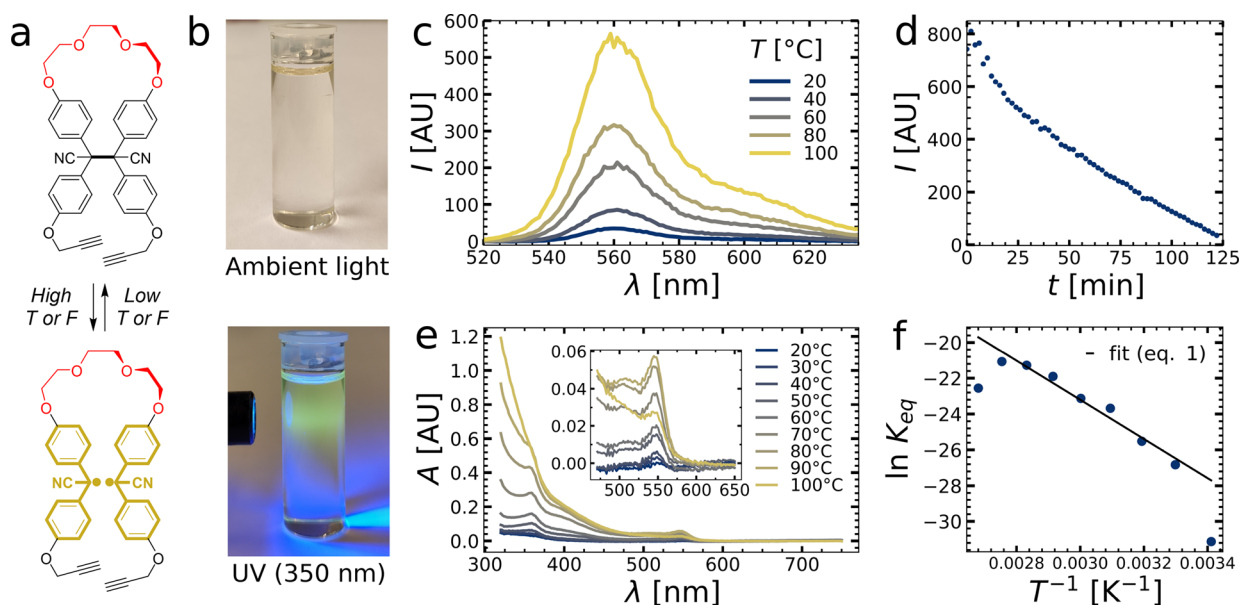


Figure 2. (a) Bridged TASN can open reversibly under thermal and mechanical triggers, yielding a yellow fluorescent radical. (b) Solutions of the bridged TASN are colorless at room temperature and appear brightly yellow fluorescent upon irradiation at 350 nm. (c) Fluorescence emission spectra with 360 nm excitation reveal an emission peak at 560 nm that increases with temperature. (d) Decay of the 560 nm fluorescence intensity over time under 360 nm excitation at 80 °C. (e) Absorbance spectra at increasing temperatures. The inset shows the enlarged region between 525 and 560 nm. (f) Van 't Hoff plot of the ring-opening equilibrium constant $\ln K_{eq}$ versus the inverse temperature. All data in this figure were collected with a 1 mg/mL bridged TASN concentration in dimethylacetamide.

used covalent mechanophores such as spiropyran.¹⁰ Moreover, TASN shows a high sensitivity to mechanical bond scission, expressed by a substantial activation length. These properties make the bridged TASN mechanophore a good candidate for the quantitative reporting of damage processes, at the lower end of relevant forces, in polymer materials.

We synthesized a bridged version of a TASN mechanophore, adapting literature procedures,^{19–21} in which a

triethylene glycol (TEG) bridge connects the two halves of the molecule (Figure 1b). Next, we incorporate this molecule **1** into a multi-mechanophore polymer **2** by means of an azide–alkyne click polymerization (Figure 1c). The resulting polymer **2** is end-capped by using lipoic acid groups, at both ends, to ensure strong anchoring onto gold-coated surfaces. For a detailed overview of synthetic procedures and analysis, we refer to the Supporting Information.

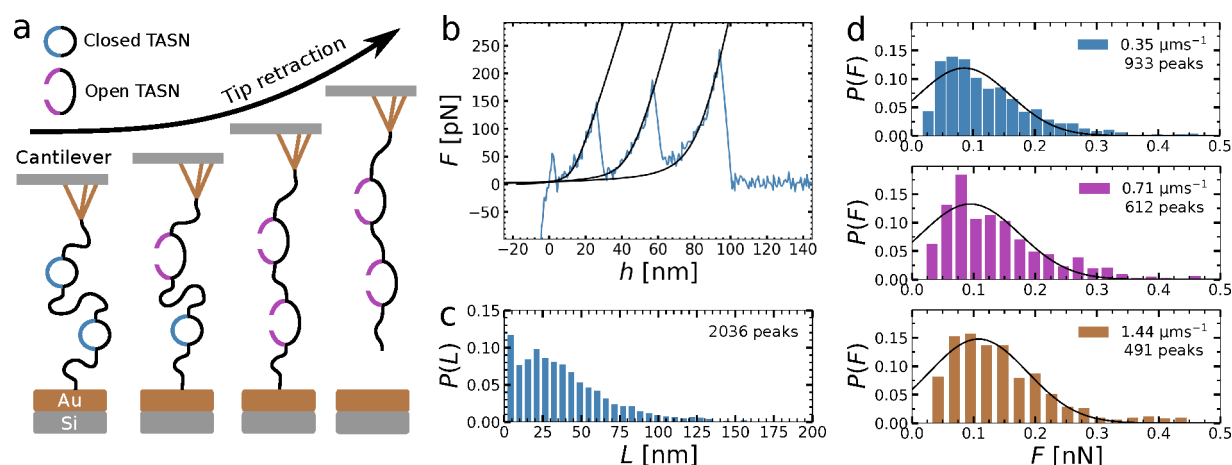


Figure 3. (a) Retracting the AFM tip stretches the mechanophore-bearing polymer, resulting in a series of sequential TASN mechanophore opening events. This continues until the lipionic acid group detaches from the gold-coated surface. (b) Typical force–extension curve showing multiple dissociation events. Extensible wormlike chain fits (eq 2) are shown in black. (c) Probability histogram of the contour length L found by the wormlike chain fits of all rupture events included in the analysis. (d) Probability histograms of the rupture forces F recorded at three tip retraction velocities (0.35, 0.71, and 1.44 $\mu\text{m s}^{-1}$). As the retraction velocity increases, the mean rupture force moves to higher forces, as indicated by Gaussian fits shown in black. The total number of peaks included in each histogram is shown in the upper right.

We first tested if the bridged TASN mechanophore **1** displays similar optical properties as the unbridged variants reported previously.¹¹ In previous studies, the reaction equilibrium between the closed and open state of TASN was found to be sensitive to temperature, shifting more toward the fluorescent open state as the temperature was increased between 20 and 100 $^{\circ}\text{C}$ (Figure 2a).¹¹

Solutions of our bridged mechanophore **1** were colorless when exposed to ambient light at room temperature, but yellow fluorescent when irradiated with a 350 nm UV lamp, indicating the presence of the activated, radical-bearing mechanophore (Figure 2b). Fluorescence spectroscopy reveals an emission peak at 560 nm (Figure 2c), also found previously for the unbridged version,¹¹ whose intensity increases upon increasing the temperature. This is in agreement with a shifting equilibrium from the closed to the open state. We note that these radical species are remarkably stable, with a half-life of 40 min at 80 $^{\circ}\text{C}$ (Figure 2d). Absorbance spectra reveal characteristic peaks at 360 and 548 nm, which also increase with increasing temperature (Figure 2e). These peaks were previously attributed to the open state of the mechanophore.¹¹ We note that at 100 $^{\circ}\text{C}$ the absorbance decreases as the result of accelerated radical quenching at high temperatures. From these data, using the extinction coefficient for TASN reported previously,¹¹ we calculate the concentration of activated mechanophore and the corresponding equilibrium constant $\ln K_{\text{eq}}$ for the equilibrium between open and closed states, which we plot as a function of the inverse temperature (Figure 2f). From a fit of these results to the van't Hoff equation

$$\ln K_{\text{eq}} = -\frac{\Delta H}{RT} + \frac{\Delta S}{R} \quad (1)$$

we can determine the reaction enthalpy ΔH and entropy ΔS , with R being the gas constant and T the absolute temperature. The first and last data points in Figure 2f strongly deviate from the trend predicted by eq 1; we excluded these two data points from the fit, as the absorbance was close to the noise level at 20 $^{\circ}\text{C}$ and notably affected by thermal degradation of the mechanophore at 100 $^{\circ}\text{C}$. We determine that $\Delta H = 91$ kJ/mol and $\Delta S = 80$ J/(K mol), resulting in reaction free energy

at 25 $^{\circ}\text{C}$ of $\Delta G = 67$ kJ/mol. Interestingly, ΔH is very close to the value of 93 kJ/mol previously reported for unbridged TASN mechanophore, whereas the entropy change ΔS is much lower compared to the 100 J/(K mol) previously reported. The lowering of the reaction entropy is attributed to the reduction in translational entropy in our bridged mechanophore upon labile bond scission. These results indicate how our bridged TASN mechanophore shows properties and reaction equilibria in full agreement with the unbridged version reported previously.¹¹

We now use single-molecule force spectroscopy, on an atomic force microscope, to evaluate the molecular mechanics of TASN activation under mechanical tension. To maximize the statistics in these single-molecule experiments, we use multi-mechanophore polymers consisting of our bridged TASN mechanophore **1** linked by ethylene glycol spacers. This approach of attaching multiple motifs in series has been used previously in single-molecule force spectroscopy experiments on supramolecular bonding motifs^{22–25} and covalent mechanophores.^{26,27}

We anchor these polymers, using their terminal lipionic acid moieties, to gold-coated surfaces and the gold-coated AFM tip. Because polymer **2** contains multiple bridged TASN mechanophores along its backbone, each force–extension curve exhibits multiple TASN activation events (Figure 3a). A typical example of a force–extension curve exhibiting multiple ruptures can be seen in Figure 3b; a large ensemble of other examples is provided in the Supporting Information.

Typically, we observe a series of nonlinear polymer stretching events, followed by a sudden drop in the force, which signals mechanophore activation. Because our measurement enforces full separation of tip from surface at the end of each approach–retract cycle, we expect that the final peak in each force–extension curve corresponds to dissociation of the lipionic acid from the gold surface rather than a mechanophore activation event. For this reason, the final peak was systematically excluded from all subsequent analysis. Further discussion on this is provided in the Supporting Information, section 4.5. We first determine characteristics of the polymer by fitting the force–extension curves prior to the rupture

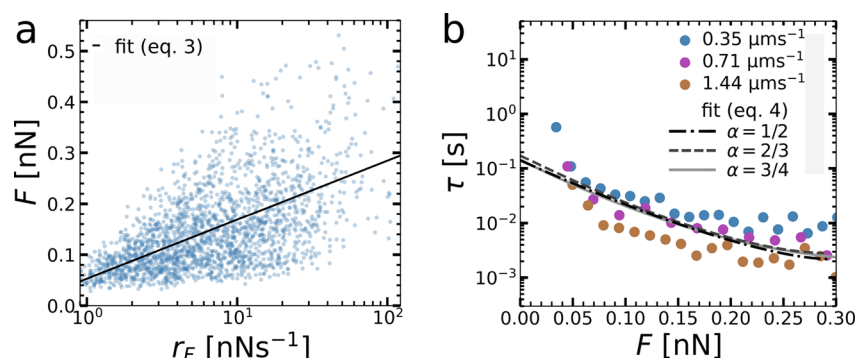


Figure 4. (a) Data cloud of the bond rupture events collected at each of the tip retraction velocities (0.35, 0.71, and 1.44 $\mu\text{m s}^{-1}$) pooled together, showing the rupture force F versus the force rate at the moment of bond rupture r_F . A Bell–Evans fit (eq 3) was plotted through the data to determine the constants k_0 and Δx^\ddagger . (b) Force–lifetime plot obtained by transforming the rupture force histograms from Figure 3d with the Dudko–Hummer–Szabo method.³⁸ Fits of eq 4 are shown for different values of the scaling factor α .

events with an approximation of the extensible wormlike chain model (eq 2)²⁸

$$\frac{FP}{k_B T} = \frac{1}{4} \left(1 - \frac{h}{L} + \frac{F}{K} \right)^{-2} - \frac{1}{4} + \frac{h}{L} - \frac{F}{K} - 0.8 \left(\frac{h}{L} - \frac{F}{K} \right)^{2.15} \quad (2)$$

in which L is the polymer contour length, P its persistence length, and K is the enthalpic compliance of the polymer. We extract these properties by fitting eq 2 to individual stretching events in our data; two examples are shown as black solid lines in Figure 3b. During the fits, we fix P at the value previously observed for poly(ethylene glycol) of 3.8 Å.^{29,30}

We performed these measurements at three tip retraction velocities: 0.35, 0.71, and 1.44 $\mu\text{m s}^{-1}$. For each velocity, we fitted at least 491 mechanophore activation events with eq 2. We find a typical contour length with an optimum in the range of 20–30 nm, as shown from L distributions shown Figure 3c.

We also determined the polymer molecular weight using gel permeation chromatography (GPC), resulting in $M_n = 4.5$ kg/mol and a polydispersity of $M_w/M_n = 2.0$ (Figure S32). On the basis of the molecular mass of the polymer, we calculated an average number of TASN mechanophore units per polymer ($\langle N \rangle$) of between 4.5 and 5.9 (Supporting Information, section 4.6). As we typically find between 1 and 4 mechanophore activation events in our force–extension curves, this indicates that not all mechanophore elements are activated before the polymer dissociates from the surface. Considering a typical covalent bond length of 1.5 Å, we can make a rough estimate of the contour length of between 26 nm for 4.5 mechanophore units and 33 nm for 5.9 mechanophore units, in good agreement with the contour lengths determined from our extensible wormlike chain fits, across all three retraction velocities (Figure S29).

We further made a distribution of the polymer extension length at the point of mechanophore activation (Figure S30), and we find that the polymers are typically stretched to a length of 20–40 nm when mechanophore activation occurs. These extension lengths are remarkably close to the contour lengths we found in the GPC analysis, which implies that the polymers are often stretched to a length close to their contour lengths. In this regime, enthalpic contributions to the force–extension behavior become important, as the polymer bonds themselves are being stretched. Such enthalpic contributions

are not accounted for by the standard wormlike chain typically used to describe the PEG force–extension behavior. For this reason, we specifically chose to analyze the force–extension curves with the extensible wormlike chain model, which accounts for the enthalpic contributions by the enthalpic compliance parameter K .

We record the dissociation force for each mechanophore activation event as the amplitude of force drop at rupture. Rupture force distributions are well described by a Gaussian shape for all three retraction velocities (Figure 3d) and show how TASN activation is peaked at forces of 100 pN, well below those reported for other covalent mechanophores studied previously.^{10,31–33} Moreover, this is an order of magnitude below the dissociation forces reported for stable C–C bonds,³⁴ further supporting the notion that the central scissile bond in TASN is very labile.

The average rupture force increases somewhat with the tip retraction velocity. This is in agreement with the Bell–Evans picture that describes mechanical bond scission as a thermally activated process whose energy landscape is tilted by the action of mechanical stress.^{35,36} To compare our data to this model, we first extract the loading rate r_F , defined as the rate of force increase at the moment of bond dissociation, from fits to the extension curve for each individual event. This results in a single point in a (r_F , F) diagram for each rupture event as shown in Figure 4a. Increasing the retraction velocity will on average lead to larger loading rates as well as larger rupture forces. To quantify this trend, we compute the rupture force and loading rate of each activation event, and we represent these events as the data cloud in Figure 4a. We then fit this data cloud with the Bell–Evans model, which predicts the following logarithmic relationship between the loading rate and the activation force:^{35,36}

$$F = \frac{k_B T}{\Delta x^\ddagger} \ln \left[\frac{\Delta x^\ddagger}{k_0 k_B T} r_F \right] \quad (3)$$

where k_0 is the zero-force bond dissociation rate and Δx^\ddagger is the activation length. The activation length defines how steeply the energy landscape tilts under mechanical stress and is thus a measure for the susceptibility of a particular mechanophore to force-induced activation. The accurate determination of these parameters requires a large amount of activation events spread over multiple orders of magnitudes of loading rates. The loading rate range we sample is somewhat limited to 2 orders of magnitude because of the limited number of retract

velocities we tested. However, because we sample a large amount of data points over this range, we can still get an estimation of the parameters k_0 and Δx^\ddagger . We find that our data are consistent with the Bell–Evans description in eq 3 (see Figure 4a) for $\Delta x^\ddagger = 0.82 \text{ \AA}$ and a zero-force dissociation rate of $k_0 = 7.0 \text{ s}^{-1}$.

On the basis of the raw data, we obtained an estimated rupture force for TASN of $\sim 100\text{--}150$, depending on the loading rate. However, since we perform our analysis on multi-mechanophore chains, the rupture probability of the first event differs from subsequent events.³⁷ A first-order correction for this effect can be done by using the approach suggested by Evans and Williams, in which the measured rupture force in a multiblock chain F_N and the rupture force of the individual mechanophore units F_1 are related as $F_N = F_1 - F_\beta \ln N$, where F_β is the thermal force and N the number of TASN subunits in the chain.³⁷ The thermal force was previously estimated to be $F_\beta \approx 20 \text{ pN}$,²⁴ and we observe $\langle N \rangle \approx 5$ as discussed above on the basis of our AFM and GPC data. This leads to a correction of $\sim +30 \text{ pN}$ on the TASN rupture force and a single-mechanophore rupture force at $130\text{--}180 \text{ pN}$, which is substantially lower than the common mechanophore spiropyran (SP),¹⁰ which exhibits a rupture force at $240\text{--}260 \text{ pN}$. Moreover, TASN has a much lower k_0 than SP, indicating a much more dynamic and weaker scissile bond, and its relatively large value for $\Delta x^\ddagger = 0.82 \text{ \AA}$ points to a good susceptibility of this mechanophore to force-induced activation, albeit less so than spiropyran for which it was reported that $\Delta x^\ddagger = 2.0 \text{ \AA}$.

Because these mechanophores exist in a dynamic equilibrium between inactive and active forms, which is shifted by the application of a force, it is instructive not only to consider a “typical” rupture force but also to study the kinetics of the conversion of the inactive to the active form. Using a theoretical framework proposed by Dudko, Hummer, and Szabo, here abbreviated the DHS method, an estimation of the change in bond lifetime with the applied force can be obtained from the force ramp experiments.³⁸ Using the DHS method, we transform the rupture force distributions (Figure 3d), having the value of r_F from the fit of the extension curve, into the force–bond lifetime curves, as shown in Figure 4b. We note that the sparse data $>300 \text{ pN}$ (Figure 3d) are not taken into account here as the number of events is too limited for an accurate conversion. We find that the data collected at the three retraction velocities collapse onto a single master curve within experimental uncertainty. This collapse of the data sets onto a single curve supports the validity of using the DHS method to obtain bond lifetime information from force-ramp experiments.³⁸ We fit the thus obtained force–lifetime curves to a modified Bell–Evans equation that takes into account the shape of the energy landscape:³⁹

$$\tau(F) = \tau_0 \left(1 - \frac{\alpha F x^\ddagger}{\Delta G^\ddagger} \right)^{1-1/\alpha} e^{-\beta \Delta G^\ddagger [1 - (1 - \alpha F x^\ddagger / \Delta G^\ddagger)^{1/\alpha}]} \quad (4)$$

Here, τ denotes the bond lifetime, with τ_0 its value at zero force, x^\ddagger is the activation length, and $\beta = 1/k_B T$. Equation 4 takes into account the shape of the energy barrier ΔG^\ddagger for mechanophore activation, through the parameter α . For a harmonic potential well with a barrier that is cusplike, $\alpha = 1/2$. For a square barrier $\alpha = 1$, and Equation 4 simplifies back to the Bell–Evans equation for the lifetime: $\tau(F) = \tau_0 \exp[-\beta F x^\ddagger]$.³⁹ To investigate the extent to which the shape of the energy barrier affects the bond lifetime, we fit Equation 4

to the force–lifetime curve for three fixed values for α (lines in Figure 4b). In general, Equation 4 gives a good description of our data set, with the exception of the low force data points recorded at $0.35 \mu\text{m s}^{-1}$. As we detected comparatively few dissociation events at forces below 50 pN and above 200 pN , we might expect our lifetime calculations to show larger errors in these regimes (Figure 3d). It should further be noted that eq 4 becomes invalid at force $F = \Delta G^\ddagger / \alpha x^\ddagger$,³⁸ where eq 4 predicts an unphysical divergence of τ . Our fits are therefore shown only in the regime before this unphysical increase occurs.

The three fits provide zero-force bond lifetimes in the range of $\tau_0 = 0.14\text{--}0.17 \text{ s}$. Mechanical tension accelerates bond dissociation, leading to lifetimes as low as 10^{-3} s at the largest forces explored of 300 pN . These lifetimes are short compared to stable covalent bonds and more comparable to supramolecular interactions,²⁴ the central succinonitrile bond in the TASN mechanophore thus behaves as a dynamic covalent bond. For the fit parameters we find for fixed values α of $1/2$, $2/3$, and $3/4$ the values $\tau_0 = 0.14$, 0.17 , and 0.14 s , $x^\ddagger = 1.0$, 0.96 , and 0.86 \AA , and $\Delta G^\ddagger = 5.9 k_B T$, $5.4 k_B T$, and $5.2 k_B T$, respectively. These results for the activation length are of the same order of magnitude as those described above. On the basis of our finding that x^\ddagger and ΔG^\ddagger are not constant across the range of α values fitted, we conclude that the kinetics of mechanophore activation are not governed by the height and position of the energy barrier alone, but its shape plays an important role as well.

The short activation time scales of the TASN mechanophore establish it as a dynamic covalent bond. These are bonds that in spite of their covalent nature can quickly switch between various states on short time scales.^{40,41} This relatively uncommon type of bond has found its uses in material science both as a way of providing useful material properties such as self-healing,^{42–44} shape memory,^{45,46} and thermal reversibility⁴⁷ and as a way of introducing sensing properties for triggers such as temperature or mechanical force.^{5,48}

Here we have conducted a detailed characterization of the force-induced mechanical activation of a tetraaryl succinonitrile (TASN) fluorescent mechanophore at the single-molecule level. Our results reveal that TASN is a useful candidate for mechanical damage reporting because of its low threshold forces for activation of $130\text{--}180 \text{ pN}$, fast bond kinetics at time scales on the order of seconds or below, large mechanical susceptibility as evidenced by its relatively large activation length, and reversibility. Previous studies have also shown how thermally or optically generated TASN radicals can be used as initiators for polymerization reactions.⁴⁹ This opens the opportunity that TASN not only can be used to report damage but also can be utilized to create chemically active radicals in response to mechanical stress in materials at low forces, which could in turn be harnessed to activate polymerizations that locally reinforce a material at a site of damage and slow down damage accumulation.⁵⁰

■ ASSOCIATED CONTENT

Supporting Information

The Supporting Information is available free of charge at <https://pubs.acs.org/doi/10.1021/acs.jpcc.1c09314>.

Organic synthesis procedures of mechanophore **1** and mechanophore-bearing polymer **2**; experimental procedures for the single-molecule force spectroscopy experiments and the optical spectroscopy experiments;

supporting data showing raw single molecule force–distance curves, an overview force–distance curves with extensible WLC fits, probability histograms of the fit parameters L and K , extension length statistics at the point of dissociation, dissociation force analysis as a function of peak order, gel permeation chromatography results, and mechanical activation of mechanophore 1 through grinding (PDF)

AUTHOR INFORMATION

Corresponding Author

Joris Sprakel – Physical Chemistry and Soft Matter, Wageningen University & Research, 6708WE Wageningen, The Netherlands; orcid.org/0000-0001-6532-4514; Email: joris.sprakel@wur.nl

Authors

Martijn van Galen – Physical Chemistry and Soft Matter, Wageningen University & Research, 6708WE Wageningen, The Netherlands; orcid.org/0000-0002-5329-4087

Jeya Prathap Kaniraj – Physical Chemistry and Soft Matter and Laboratory of Organic Chemistry, Wageningen University & Research, 6708WE Wageningen, The Netherlands

Bauke Albada – Laboratory of Organic Chemistry, Wageningen University & Research, 6708WE Wageningen, The Netherlands; orcid.org/0000-0003-3659-2434

Complete contact information is available at: <https://pubs.acs.org/10.1021/acs.jpcc.1c09314>

Author Contributions

M.v.G. and J.P.K. contributed equally to this work.

Notes

The authors declare no competing financial interest.

ACKNOWLEDGMENTS

The authors thank Prof. Hideyuki Otsuka for valuable discussions. The research presented in this article was financially supported by VLAG Graduate School. This work was part of the VIDi research program of J.S. (project no. 723.016.001), which was financed by the NWO. This project has received funding from the European Research Council (ERC) under the European Union's Horizon 2020 research and innovation programme (grant agreement no. 101000981)

REFERENCES

- (1) Davis, D. A.; Hamilton, A.; Yang, J.; Cremer, L. D.; van Gough, D.; Potisek, S. L.; Ong, M. T.; Braun, P. V.; Martinez, T. J.; White, S. R.; et al. Force-induced activation of covalent bonds in mechanoresponsive polymeric materials. *Nature* **2009**, *459*, 68–72.
- (2) Robb, M. J.; Kim, T. A.; Halmes, A. J.; White, S. R.; Sottos, N. R.; Moore, J. S. Regioisomer-Specific Mechanochromism of Naphthopyran in Polymeric Materials. *J. Am. Chem. Soc.* **2016**, *138*, 12328–12331.
- (3) Versaw, B. A.; McFadden, M. E.; Husic, C. C.; Robb, M. J. Designing naphthopyran mechanophores with tunable mechanochromic behavior. *Chem. Sci.* **2020**, *11*, 4525–4530.
- (4) Wang, Z.; Ma, Z.; Wang, Y.; Xu, Z.; Luo, Y.; Wei, Y.; Jia, X. A Novel Mechanochromic and Photochromic Polymer Film: When Rhodamine Joins Polyurethane. *Adv. Mater.* **2015**, *27*, 6469–6474.
- (5) Chen, Y.; Mellot, G.; van Luijk, D.; Creton, C.; Sijbesma, R. P. Mechanochemical tools for polymer materials. *Chem. Soc. Rev.* **2021**, *50*, 4100.
- (6) Ducrot, E.; Chen, Y.; Bulters, M.; Sijbesma, R. P.; Creton, C. Toughening Elastomers with Sacrificial Bonds and Watching Them Break. *Science* **2014**, *344*, 186–189.
- (7) Wang, T.; Zhang, N.; Dai, J.; Li, Z.; Bai, W.; Bai, R. Novel Reversible Mechanochromic Elastomer with High Sensitivity: Bond Scission and Bending-Induced Multicolor Switching. *ACS Appl. Mater. Interfaces* **2017**, *9*, 11874–11881.
- (8) Hoshino, F.; Kosuge, T.; Aoki, D.; Otsuka, H. Mechano-fluorescent polymer/silsesquioxane composites based on tetraarylsuccinonitrile. *Mater. Chem. Front.* **2019**, *3*, 2681–2685.
- (9) Chen, Y.; Yeh, C. J.; Qi, Y.; Long, R.; Creton, C. From force-responsive molecules to quantifying and mapping stresses in soft materials. *Sci. Adv.* **2020**.
- (10) Gosswiler, G. R.; Kouznetsova, T. B.; Craig, S. L. Force-Rate Characterization of Two Spiropyran-Based Molecular Force Probes. *J. Am. Chem. Soc.* **2015**, *137*, 6148–6151.
- (11) Sumi, T.; Goseki, R.; Otsuka, H. Tetraarylsuccinonitriles as mechanochromophores to generate highly stable luminescent carbon-centered radicals. *ChemComm* **2017**, *53*, 11885–11888.
- (12) Ishizuki, K.; Aoki, D.; Goseki, R.; Otsuka, H. Multicolor Mechanochromic Polymer Blends That Can Discriminate between Stretching and Grinding. *ACS Macro Lett.* **2018**, *7*, 556–560.
- (13) Kato, S.; Ishizuki, K.; Aoki, D.; Goseki, R.; Otsuka, H. Freezing-Induced Mechanoluminescence of Polymer Gels. *ACS Macro Lett.* **2018**, *7*, 1087–1091.
- (14) Kato, S.; Furukawa, S.; Aoki, D.; Goseki, R.; Oikawa, K.; Tsuchiya, K.; Shimada, N.; Maruyama, A.; Numata, K.; Otsuka, H. Crystallization-induced mechanofluorescence for visualization of polymer crystallization. *Nat. Commun.* **2021**, *12*, 126.
- (15) Chen, Y.; Spiering, A. J. H.; Karthikeyan, S.; Peters, G. W. M.; Meijer, E. W.; Sijbesma, R. P. Mechanically induced chemiluminescence from polymers incorporating a 1,2-dioxetane unit in the main chain. *Nat. Chem.* **2012**, *4*, 559–562.
- (16) Chen, Y.; Sijbesma, R. P. Dioxetanes as Mechanoluminescent Probes in Thermoplastic Elastomers. *Macromolecules* **2014**, *47*, 3797–3805.
- (17) Kabb, C. P.; O'Bryan, C. S.; Morley, C. D.; Angelini, T. E.; Sumerlin, B. S. Anthracene-based mechanophores for compression-activated fluorescence in polymeric networks. *Chem. Sci.* **2019**, *10*, 7702–7708.
- (18) Church, D. C.; Peterson, G. I.; Boydston, A. J. Comparison of Mechanochemical Chain Scission Rates for Linear versus Three-Arm Star Polymers in Strong Acoustic Fields. *ACS Macro Lett.* **2014**, *3*, 648–651.
- (19) Katritzky, A.; Belyakov, S.; Denisko, O.; Maran, U.; Dalal, N. New podands with terminal chromogenic moieties derived from formazans. *J. Chem. Soc., Perkin Trans. 2* **1998**, 611–615.
- (20) Malona, J. A.; Cariou, K.; Spencer, W. T., III; Frontier, A. J. Total Synthesis of (\pm)-Rocaglamide via Oxidation-Initiated Nazarov Cyclization. *J. Org. Chem.* **2012**, *77*, 1891–1908.
- (21) Shi, L.; Jing, C.; Ma, W.; Li, D.-W.; Halls, J. E.; Marken, F.; Long, Y.-T. Plasmon Resonance Scattering Spectroscopy at the Single-Nanoparticle Level: Real-Time Monitoring of a Click Reaction. *Angew. Chem. Int.* **2013**, *52*, 6011–6014.
- (22) Zou, S.; Schönherr, H.; Vancso, G. J. Stretching and Rupturing Individual Supramolecular Polymer Chains by AFM. *Angew. Chem. int. ed.* **2005**, *44*, 956–959.
- (23) Liu, Y.; Yu, Y.; Gao, J.; Wang, Z.; Zhang, X. Water-Soluble Supramolecular Polymerization Driven by Multiple Host-Stabilized Charge-Transfer Interactions. *Angew. Chem. int. ed.* **2010**, *49*, 6576–6579.
- (24) Embrechts, A.; Schönherr, H.; Vancso, G. J. Rupture force of single supramolecular bonds in associative polymers by AFM at fixed loading rates. *J. Phys. Chem. B* **2008**, *112*, 7359–7362.
- (25) Embrechts, A.; Schönherr, H.; Vancso, G. J. Forced Unbinding of Individual Urea-Aminotriazine Supramolecular Polymers by Atomic Force Microscopy: A Closer Look at the Potential Energy Landscape and Binding Lengths at Fixed Loading Rates. *J. Phys. Chem. B* **2012**, *116*, 565–570.

- (26) Bowser, B. H.; Craig, S. L. Empowering mechanochemistry with multi-mechanophore polymer architectures. *Polym. Chem.* **2018**, *9*, 3583–3593.
- (27) Klukovich, H. M.; Kouznetsova, T. B.; Kean, Z. S.; Lenhardt, J. M.; Craig, S. L. A backbone lever-arm effect enhances polymer mechanochemistry. *Nat. Chem.* **2013**, *5*, 110–114.
- (28) Petrosyan, R. Improved approximations for some polymer extension models. *Rheol. Acta* **2017**, *56*, 21–26.
- (29) Lee, H.; Venable, R. M.; MacKerell, A. D.; Pastor, R. W. Molecular Dynamics Studies of Polyethylene Oxide and Polyethylene Glycol: Hydrodynamic Radius and Shape Anisotropy. *Biophys. J.* **2008**, *95*, 1590–1599.
- (30) Kienberger, F.; Pastushenko, V. P.; Kada, G.; Gruber, H. J.; Riener, C.; Schindler, H.; Hinterdorfer, P. Static and Dynamical Properties of Single Poly(Ethylene Glycol) Molecules Investigated by Force Spectroscopy. *Single Mol.* **2000**, *1*, 123–128.
- (31) Yao, R.; Li, X.; Xiao, N.; Weng, W.; Zhang, W. Single-molecule observation of mechanical isomerization of spirothiopyran and subsequent Click addition. *Nano Res.* **2021**, *14*, 2654–2658.
- (32) Horst, M.; Yang, J.; Meisner, J.; Kouznetsova, T. B.; Martínez, T. J.; Craig, S. L.; Xia, Y. Understanding the Mechanochemistry of Ladder-Type Cyclobutane Mechanophores by Single Molecule Force Spectroscopy. *J. Am. Chem. Soc.* **2021**, *143*, 12328–12334.
- (33) Schütze, D.; Holz, K.; Müller, J.; Beyer, M. K.; Lüning, U.; Hartke, B. Pinpointing Mechanochemical Bond Rupture by Embedding the Mechanophore into a Macrocyclic. *Angew. Chem., Int. Ed.* **2015**, *54*, 2556–2559.
- (34) Grandbois, M.; Beyer, M.; Rief, M.; Clausen-Schaumann, H.; Gaub, H. How strong is a covalent bond? *Science* **1999**, *283*, 1727–1730.
- (35) Bell, G. Models for the specific adhesion of cells to cells. *Science* **1978**, *200*, 618–627.
- (36) Evans, E.; Ritchie, K. Dynamic strength of molecular adhesion bonds. *Biophys. J.* **1997**, *72*, 1541–1555.
- (37) Evans, E.; Williams, P. Dynamic Force Spectroscopy. Physics of bio-molecules and cells. In *Physique des biomolécules et des cellules*; Berlin, 2002; pp 145–204.
- (38) Dudko, O. K.; Hummer, G.; Szabo, A. Theory, analysis, and interpretation of single-molecule force spectroscopy experiments. *Proc. Natl. Acad. Sci. U. S. A.* **2008**, *105*, 15755–15760.
- (39) Dudko, O.; Hummer, G.; Szabo, A. Intrinsic rates and activation free energies from single-molecule pulling experiments. *Phys. Rev. Lett.* **2006**, *96*, 108101.
- (40) Chakma, P.; Konkolewicz, D. Dynamic Covalent Bonds in Polymeric Materials. *Angew. Chem., Int. Ed.* **2019**, *58*, 9682–9695.
- (41) Maeda, T.; Otsuka, H.; Takahara, A. Dynamic covalent polymers: Reorganizable polymers with dynamic covalent bonds. *Prog. Polym. Sci.* **2009**, *34*, 581–604.
- (42) Deng, G.; Tang, C.; Li, F.; Jiang, H.; Chen, Y. Covalent cross-linked polymer gels with reversible sol-gel transition and self-healing properties. *Macromolecules* **2010**, *43*, 1191–1194.
- (43) Roy, N.; Bruchmann, B.; Lehn, J.-M. DYNAMERS: dynamic polymers as self-healing materials. *Chem. Soc. Rev.* **2015**, *44*, 3786–3807.
- (44) Zhang, Z. P.; Rong, M. Z.; Zhang, M. Q.; Yuan, C. Alkoxyamine with reduced homolysis temperature and its application in repeated autonomous self-healing of stiff polymers. *Polym. Chem.* **2013**, *4*, 4648–4654.
- (45) Wang, Y.; Pan, Y.; Zheng, Z.; Ding, X. Reconfigurable and Reprocessable Thermoset Shape Memory Polymer with Synergetic Triple Dynamic Covalent Bonds. *Macromol. Rapid Commun.* **2018**, *39*, 1800128.
- (46) Miao, W.; Zou, W.; Jin, B.; Ni, C.; Zheng, N.; Zhao, Q.; Xie, T. On demand shape memory polymer via light regulated topological defects in a dynamic covalent network. *Nat. Commun.* **2020**, *11*, 1–8.
- (47) Chen, X.; Dam, M. A.; Ono, K.; Mal, A.; Shen, H.; Nutt, S. R.; Sheran, K.; Wudl, F. A thermally re-mendable cross-linked polymeric material. *Science* **2002**, *295*, 1698–1702.
- (48) Kato, S.; Aoki, D.; Otsuka, H. Postmodification of Polymer Networks via the Freezing-Induced Generation of Radicals. *ACS Appl. Polym. Mater.* **2021**, *3*, 594–598.
- (49) Braun, D.; SteinhauerBeisser, S. Initiation of polymerization with substituted ethanes 0.15. Telomerization of methacrylate monomers with tetraphenyl succinonitrile. *Eur. Polym. J.* **1997**, *33*, 7–12.
- (50) Matsuda, T.; Kawakami, R.; Namba, R.; Nakajima, T.; Gong, J. P. Mechanoresponsive self-growing hydrogels inspired by muscle training. *Science* **2019**, *363*, 504.